Journal of Solid State Chemistry 187 (2012) 97–102

Contents lists available at SciVerse ScienceDirect

Journal of Solid State Chemistry

journal homepage: www.elsevier.com/locate/jssc

Organized thiol functional groups in mesoporous core shell colloids

Martín H. Marchena [a,1], Mara Granada [b,c], Andrea V. Bordoni [a], María Joselevich [d], Horacio Troiani [b,c], Federico J. Williams [e], Alejandro Wolosiuk [a,*]

[a] Gerencia Química, Centro Atómico Constituyentes, Comisión Nacional de Energía Atómica (CNEA), Avda. Gral. Paz 1499, B1650KNA Buenos Aires, Argentina
[b] Centro Atómico Bariloche—CNEA, 8400 San Carlos de Bariloche, Argentina
[c] Instituto Balseiro—Centro Atómico Bariloche—CNEA, San Carlos de Bariloche 8400, Argentina
[d] Asociación Civil Expedición Ciencia, Cabrera 4948, C1414BGP Buenos Aires, Argentina
[e] DQIAQyF—INQUIMAE FCEN, Universidad de Buenos Aires, Ciudad Universitaria, Pabellón II, C1428EHA Buenos Aires, Argentina

ARTICLE INFO

Article history:
Received 7 October 2011
Received in revised form
20 December 2011
Accepted 23 December 2011
Available online 4 January 2012

Keywords:
Mesoporous silica
Colloids
Templated materials
Core–shell
Thiols

ABSTRACT

The co-condensation *in situ* of tetraethoxysilane (TEOS) and mercaptopropyltrimethoxysilane (MPTMS) using cetyltrimethylammonium bromide (CTAB) as a template results in the synthesis of multilayered mesoporous structured SiO_2 colloids with "onion-like" chemical environments. Thiol groups were anchored to an inner selected SiO_2 porous layer in a bilayered core shell particle producing different chemical regions inside the colloidal layered structure. X-Ray Photoelectron Spectroscopy (XPS) shows a preferential anchoring of the –SH groups in the double layer shell system, while porosimetry and simple chemical modifications confirm that pores are accessible. We can envision the synthesis of interesting colloidal objects with defined chemical environments with highly controlled properties.

1. Introduction

The synthesis of core–shell nanoparticles and colloids represents a new field in combining inorganic and organic chemistry synthesis and biological chemistry in the design of new objects [1]. A colorful materials "palette" from inorganic oxides to soft matter polymers, metals to semiconductors, enzymes and proteins stand as building blocks materials for the synthesis of complex nanometric and colloidal particles. In addition, colloidal layered structures such as core–shell colloids have received considerable attention due to their interesting properties as entities with tailored physical and chemical properties: controlled refractive index and plasmonic structures [2], chemical and biochemical reactors [3], sensors and responsive materials [4], biological labels and tribological tracers [5], abrasives [6], artificial cells [7] and nanocapsules [8]. In addition, core–shell structures after appropriate etching chemistry result in hollow objects or "nanorattle" systems [9]. In this context, layered materials present unique opportunities for building supramolecular architectures with highly controlled chemistry and environments [10–12]. Applications in catalysis and sorbent materials take advantage of the high area/volume ratios in mesoporous nanoparticles while rational synthesis of the core and the porous shell results in hierarchical integrated chemical systems [13]. Indeed, mesoporous layers or shells are excellent molecular frameworks for analyte transport and diffusion or the transduction of chemical or physical events [14,15]. Also, with their higher loading capacities, due to the increased surface area, mesoporous silica particles have a great potential as drug delivery carriers. Indeed, silica is considered as a safe material in terms of biocompatibility with low cytotoxicity and high chemical stability [16a]. In this context, Zink et al. synthesized mesoporous SiO_2 load cargo molecules with responsive pores based on pH and light "switches" that released therapeutic agents [16b,c]. This perspective has opened an exciting field known as *theranostic medicine* where submicrometric objects include high density chemical functions for sensing, labeling and treating diseases [16a].

Usually, mesoporous materials rely on the use of soft templates such as surfactants for pore generation in the 2–15 nm range [17] while shell synthesis can be performed either under liquid phase or aerosol depositions or a combination of both techniques [18]. Sol–gel alkoxide co-condensation *in situ* allows introducing chemical functionalities in the different layers or shells while post-grafting methods lack spatial localization control albeit achieving higher group densities [19]. Despite that the sequential co-condensation approach for shell deposition is highly attractive; several questions arise regarding the precise

* Corresponding author. Fax: +54 11 6772 7886.
E-mail address: wolosiuk@cnea.gov.ar (A. Wolosiuk).
[1] Present address: Gerencia de Área de Energía Nuclear—Centro Atómico Constituyentes—CNEA, Av. Gral Paz 1499, B1650KNA Buenos Aires, Argentina.

0022-4596/$ - see front matter © 2012 Elsevier Inc. All rights reserved.
doi:10.1016/j.jssc.2011.12.028

localization of the chemical groups introduced or the accessibility. Recently, Bein and coworkers [14b] illustrated in multiple core shell particles the pore accessibility and functional group localization of fluorescein isothiocyanate using fluorescence quenching by Au nanoparticles.

In this work, we present a layered core shell particle with tailored accessible thiol chemical groups in a colloidal SiO_2 mesoporous structure synthesized at room temperature. The sequential deposition of SiO_2 layers in the presence of a porogen under basic conditions permits a simple construction in a "one pot" manner. Based on the synthesis proposed by Yoon et al. and Sánchez modifications [20,21], precise localization of chemical groups within multilayered structures aims to develop hierarchical integrated chemical systems with organized supramolecular structures. Using XPS surface analysis we studied in detail the presence of thiol groups in the SiO_2 mesoporous shells along the synthetic steps and verified that these groups can be chemically modified too.

2. Experimental

2.1. Preparation of SiO_2 cores

Monodisperse solid cores were obtained by the Stöber method [22] from a mixture of ammonia, water and tetraethoxysilane. Typically, we prepared these particles mixing 784 g of ethanol, 39.9 ml of aqueous ammonia, 80.4 ml of H_2O, and 66 ml of TEOS under vigorous stirring.

2.2. Preparation of mesoporous core shell colloids

Core–shell multilayed particles were obtained by using the solid core previously obtained. Mesoporous SiO_2 layers were deposited from pure tetraethoxysilane (TEOS) or a combination of TEOS and mercaptopropyltrimethoxysilane (MPTMS) and cetyltrimethylammonium bromide as porogen (CTAB). To form the functionalized mesoporous shell, 0.06 g of solid cores were dispersed in 63 ml of deionized H_2O, 21.2 g of ethanol, 1.3 ml of aqueous ammonia and 9.1 ml of CTAB solution (110 mM, dissolved in H_2O). After stirring for 30 min, 0.60 ml of the precursors (TEOS:MPTMS 0.9:0.1 or 0.5:0.5 M ratios) were added under vigorous stirring. Typically, MPTMS/TEOS mixtures were added simultaneously after 30 min stirring drop by drop. The reaction mix was stirred at room temperature for 24 h. To form a second SiO_2 mesoporous shell, 10 ml of CTAB 110 mM and 0.45 ml of TEOS were added and the reaction mix was stirred for another 24 h.

The as synthetized samples were centrifuged and washed in an ethanolic solution prepared from 0.2 ml HCl 37% w/w in 250 ml absolute ethanol in order to remove the surfactant. This process was repeated at least five times.

All reactants were obtained from Sigma-Aldrich® and used without further purification and water was obtained from a Millipore® system (18 $M\Omega\,cm^{-1}$).

For clarity, we will omit in the particle nomenclature the dense SiO_2 core seed and we will refer, for example, to SiO_2–$SH_{x=0.1}/SiO_2$, $_{MP}$ as colloids with a thiol modified mesoporous SiO_2 middle layer with 10% by mol of MPTMS during cohydrolysis and a bare non-modified mesoporous SiO_2 outer layer.

2.3. Characterization

2.3.1. X-ray photoelectron spectroscopy (XPS)

X-ray photoelectron spectroscopy (XPS) measurements were obtained using a Specs Sage 150 spectrometer equipped with a dual anode Mg/Al X-ray source and an hemispherical electron energy analyzer. Spectra were acquired using un-monochromatic Mg$K\alpha$ (1253.6 eV) source with a 90° detection angle. Quoted binding energies (BEs) are referred to the adventitious C 1*s* emission at 285 eV. Measurements conducted over powdered samples were made by placing a drop of a concentrated suspension of colloidal particles on a gold surface and drying in air. Atomic ratios were calculated from the integrated intensities of core levels after instrumental and photoionization cross-section corrections. Shift due to electrostatic charge of the sample was corrected using C 1*s* peak as reference. In order to compare different samples, the acquired spectra were normalized using the intensity of Si 2*p* as reference.

2.3.2. Transmission and field-emission scanning electron microscopy (TEM and FE-SEM)

TEM images were obtained from a CM 200 Philips high-resolution transmission electron microscope equipped with an ultra twin objective lens and an acceleration voltage of 200 kV. Samples were deposited from ethanolic dispersions on carbon coated copper grids and dried for 24 h at room temperature. Shell thicknesses were estimated from the micrographs using ImageJ (NIH) for image analysis

Field Emission-Scanning Electron Microscopy (FE-SEM) images were taken with a ZEISS LEO 982 GEMINI field emission electron microscope in the secondary-electron mode, using an in-lens detector to improve resolution. Energy dispersive spectra (EDS) were obtained using a SEM Philips 515; samples were prepared by depositing particles onto a carbon tape.

2.3.3. Low angle X-ray diffraction (XRD)

Low-angle XRD patterns were collected in a Siemens D-5000 diffractometer using the graphite-filtered Cu$K\alpha$ radiation ($\lambda = 1.5406$ Å).

2.3.4. FT-IR

Diffuse reflectance infrared Fourier transform spectroscopy measurements (DRIFTS) were performed on a Nicolet Magna 560 instrument, equipped with a liquid nitrogen-cooled MCT-A detector. DRIFTS measurements were performed by depositing colloidal samples on a KBr filled DRIFTS sample holder. SiO_2 colloidal particles were dried for 8 h at 60 °C and 16 h at 130 °C.

2.3.5. Porosimetry

N_2 adsorption and desorption isotherms were measured at 77 K on a Micromeritics ASAP 2020 system. The specific surface area and the pore size distribution were calculated using the BET and Barrett–Jonyner–Halenda (BJH) methods.

3. Results and discussion

Silica has a great potential for entrapment of interesting species such as colloids, nanoparticles and biomolecules [3] and is an excellent material for composite synthesis [23]. In this work, dense silica core particles ranging 130–150 nm in diameter were synthesized through the Stöber approach [22] and used as seeds. From here, sequential deposition of SiO_2 layers under controlled precipitation conditions leads to designed core–shell silica structures [24]. Scheme 1 depicts the synthesis of radially organized mesoporous bishell colloids.

After the first porous layer is synthesized cohydrolyzing TEOS and MPTMS, TEM images in Fig. 1a show circular objects with a decreased electronic contrast around the SiO_2 dense cores due to the porous nature of the shell. Shell thickness can be easily controlled using different amounts of alkoxysilane, concentration

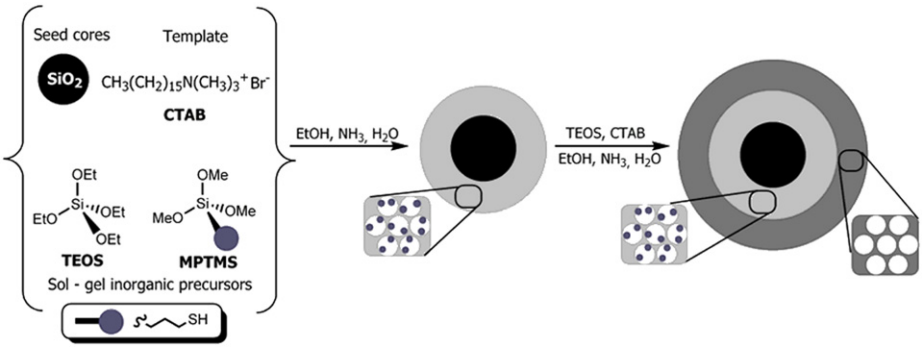

Scheme 1. Scheme for synthesis of double shell mesoporous colloids.

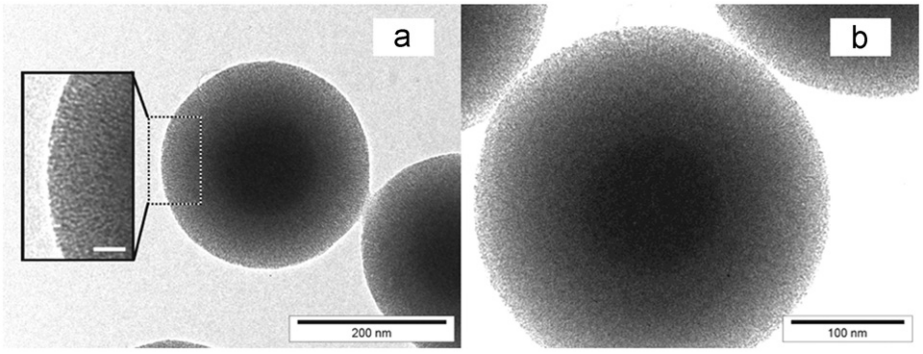

Fig. 1. TEM images: (a) SiO_2–$SH_{x=0.5}$ and (b) SiO_2–$SH_{x=0.5}$/$SiO_{2,\ MP}$. Inset scale bar=20 nm.

of seed cores, hydrolysis time and/or pore structuring agent. This flexibility is highly attractive in different synthetic schemes as liquid phase alkoxide sol–gel condensations can be carried out at room temperature and under mild chemical environments. Close inspection of the pore size in Fig. 1a suggests diameters around 2–3 nm which agrees very well with CTAB micelle size [25] while the uniform mesoporous shell thickness is around 75 nm. Moreover, there is an apparent ordered pore arrangement along the radial direction as previously observed in the literature [20,21]. This is consistent with the CTAB directed synthesis of mesoporous silicate particles observed by other researchers [26]. The condensation of silica-encapsulated cylindrical CTAB micelles results in a mesoporous silica particle with a hexagonal close-packed cylindrical pores structure [26b]. However, competition between hydrolysis and condensation reactions of TEOS and self-assembly with CTAB micelles impacts the long range order of the mesostructure. Usually, this kind of materials requires thermal treatments in order to improve the "pore crystallinity". It is likely that there is a high degree of wormholes within the SiO_2 shells synthesized in this work. We have to consider that SiO_2 shells were obtained at room temperature and with no further thermal treatment in order to not compromise the stability of the thiol groups. Further deposition of a new SiO_2 mesoporous ($SiO_{2,\ MP}$) layer on top of the first porous layer using TEOS alone keeps the spherical shape of the seed colloids as seen in Fig. 1b. In particular, this second SiO_2 mesoporous shell has 40 nm thickness and retains the porosity too. Typically, bulk SiO_2 alkoxide sol–gel materials densities range in the 2.2–1.6 g/cm^3 [19b]. This value decreases significantly when templated with CTAB or other surfactants [11], being the reason why we can differentiate between the SiO_2 core (seed particle, non-templated SiO_2) and the first porous layer in Fig. 1a. When adding a second porous layer we still see the SiO_2 core seed particle. As each porous layer is based on the same material (SiO_2) and using the same template (CTAB) we do not expect to make a distinction between them

Table 1
Porous properties calculated from N_2 adsorption isotherms for thiol-functionalized and non-functionalized mesoporous shell colloids on SiO_2 dense core colloids.

Sample	Area BET ($m^2\ g^{-1}$)	Pore diameter (nm)	Pore volume ($cm^3\ g^{-1}$)
SiO_2–$SH_{x=0.1}$	599	2.1	0.32
SiO_2–$SH_{x=0.1}$/$SiO_{2,\ MP}$	735	2.5	0.48
$SiO_{2,\ MP}$	863	2.3	0.51

using regular TEM. Nonetheless, N_2 adsorption experiments in Table 1 shows that these pores are also accessible with typical values corresponding to mesoporous materials. Again, pore diameters agree very well with CTAB micelle size confirming the TEM observations with little difference in pore size when different architectures are synthesized. The high specific surface areas obtained are attractive for catalysis and separation procedures [8,27].

We can get more information about the pore order within the different shells employing low angle XRD. Particularly, the relation between surfactant:silica molar ratio (CTAB:Si) in the synthesis of mesoporous SiO_2 determines the pore arrangement in the porous shell. When this ratio is approximately 0.5, an hexagonal phase is expected; while when CTAB:Si is near 1, cubic or lamellar phases are obtained [28]. Then, at the ratios employed in this work (CTAB:Si, 0.4) it is likely the pores are arranged in an hexagonal order. XRD measurements show a distinctive broad peak for the $\langle 1\,0\,0 \rangle$ plane when colloids have a capping mesoporous –SH terminal group as depicted in Fig. 2a. This peak corresponds to a *d* spacing of 3.01 nm accounting for the pore–center distance and can be related to the pore size and wall thickness. The *d* spacing shifts to 3.44 nm when capping the –SH layer with an outer

unmodified SiO_2 mesoporous layer. These observations agree very well with the previous TEM images were pore order was apparent. In addition there is a hint of hexagonal order induced by the CTAB micelles in the appearance of a broad peak in the region of ⟨1 1 0⟩. However, we do not observe sharp higher order reflections (e.g. ⟨2 0 0⟩) expected for hexagonal close-packed cylindrical pores. As previously observed by Tan and Rankin a possible explanation for the absence of higher order reflections is that the ordered mesopores do not form large diffraction domains as they are in thin and curved shells [26b]. Yano et al. reported the synthesis of highly ordered pores in similar systems when using methanol and tetramethoxysilane as silica source under slightly different synthetic conditions [29]. Pore size and pore–pore distances are highly dependent on thermal treatments (i.e. calcinations) in addition to the fact that radial alignment and local order of the cylindrical micelles is influenced by surface curvature and topological frustrations [30]. Besides, sol–gel SiO_2 surfactant templated materials syntheses are kinetically controlled leading to solids with amorphous inorganic pore walls [31]. However, employing the same synthetic scheme for obtaining mesoporous TiO_2, ZrO_2 or SnO_2 can result in crystalline materials after appropriate thermal treatment [31]. Nevertheless, increasing crystal size compromises the pore wall thickness and the continuous mesoporous structure leading to a fragile packing of nanocrystallites [32].

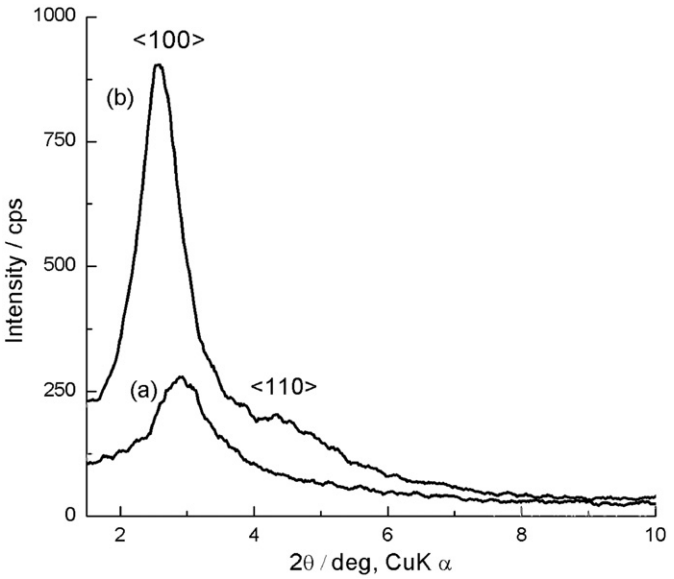

Fig. 2. Low angle XRD patterns for: (a) SiO_2–$SH_{x=0.5}$ and (b) SiO_2–$SH_{x=0.5}/SiO_{2,\ MP}$.

The FTIR of the $SiO_2/SiO_{2,\ MP}$ nanoparticles showed an intense band at 3600–3100 cm^{-1}, assigned to O–H, in addition with a large band observed at 1100–1000 cm^{-1} associated to typical Si–O and O–Si–O vibrations. Non-calcined SiO_2 sol–gel films exhibit a strong O–H stretching peak at 3400 cm^{-1} where hydrogen bonded adsorbed water has an important role [33]. Also, the 3000–3800 cm^{-1} region includes O–H stretching from silanols (isolated SiOH (3750 cm^{-1}), geminal SiOH (3742 cm^{-1}) and vicinal SiOH (3720–3520 cm^{-1})) [33]. In the FTIR spectra of the SiO_2/SiO_2–SH nanoparticles the characteristics band of aliphatic ν_{C-H} at 2900–2800 cm^{-1} was observed due the incorporation of the propyl group to the framework (Fig. 3). Raising the molar ratio of MPTMS/TEOS in the synthesis resulted in an increase in the intensity. On the other hand, S–H stretching of the thiol group usually has weak absorption signal between 2500 and 2600 cm^{-1} and shows up when $x=0.5$.

It is highly significative that water adsorption can be easily monitored inspecting the water bands (3600–3100 cm^{-1} ν_{O-H}, 1630–1600 cm^{-1} δ_{H-O-H} not shown in the figure). By increasing MPTMS/TEOS ratios, the absorption bands associated to water vibrational modes showed lower intensity, which is not surprinsing considering the hydrophobicity of the mercaptopropyl groups.

While infrared spectroscopy accounts for the presence of chemical groups in the entire colloidal structure, X-ray Photoelectron Spectroscopy (XPS) is an exceptional tool in order to evaluate the spatial localization of SH groups on the colloidal surface interface. Typical XPS surface depth detection ranges in the order of 5–10 nm according to the porosity of the material [34]. Then, we expect to analyze only the outermost layers of the mesoporous colloidal particles.

Fig. 4 shows XPS spectra of four samples where the position of thiolated layer and the concentration of –SH groups are changed. Spectra (a) and (b) correspond to particles with –SH functional groups in the outer shell and with 50% and 10% molar concentration of MPTMS, respectively, whereas spectra (c) and (d) correspond to particles with –SH groups in the inner shell also with 50% and 10% concentration, respectively. In all cases we observe two signals, one at 163.3 eV corresponding to S 2*p* due to the –SH groups and the other at 153.8 eV corresponding to Si 2*s* due to SiO_2 (http://srdata.nist.gov/xps). Clearly, as the MPTMS content during co-hydrolysis with TEOS increases from 10% to 50% (spectra (b) and (a)) there is an increase in the S 2*p* signal and

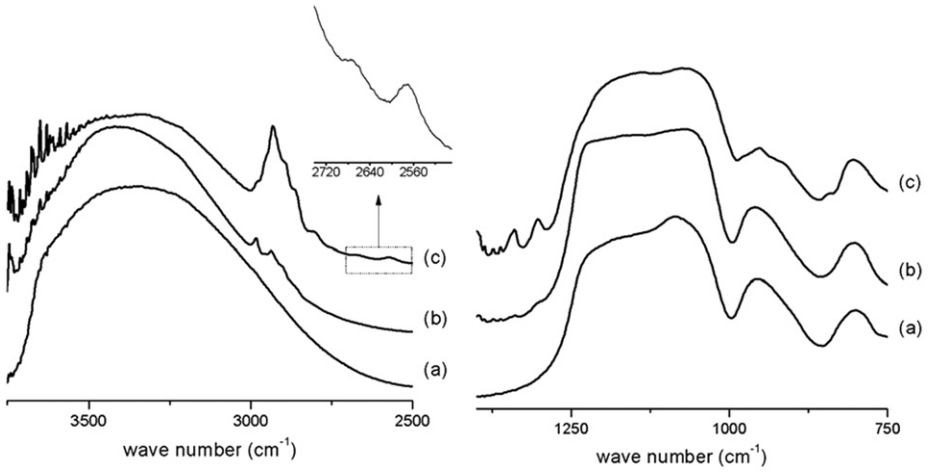

Fig. 3. FTIR spectra: (a) SiO_2 colloids, (b) SiO_2/SiO_2–$SH_{x=0.1}$, and (c) SiO_2/SiO_2–$SH_{x=0.5}$.

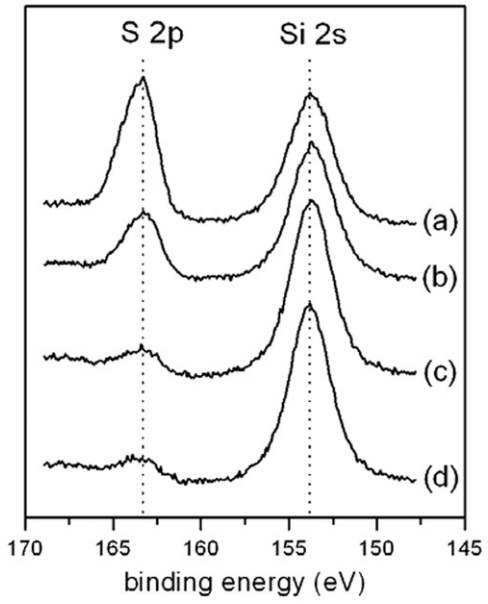

Fig. 4. XPS spectra corresponding to: (a) SiO_2–$SH_{x=0.5}$, (b) SiO_2–$SH_{x=0.1}$, (c) SiO_2–$SH_{x=0.5}/SiO_{2,\ MP}$ and (d) SiO_2–$SH_{x=0.1}/SiO_{2,\ MP}$.

a corresponding decrease in the Si 2*s* signal. Moreover, no detectable oxidized species like $-SO_3^-$ (169 eV) or –SS– (168.8 eV) are present. On the other hand, when the –SH groups are present in a middle shell (spectra (c) and (d)) the S detected is barely above the signal to noise ratio (3:1) while the Si signal is maximum. Both S signals remain the same independent of MPTMS concentration during co-condensation which could be attributed to contamination or dissolution/reprecipitation of the layers in the synthetic conditions. Therefore, the XPS data demonstrates that the position and the concentration of the –SH functional groups within the core shell mesoporous particle can be highly controlled. Besides, these groups can be chemically modified to Brønstead sulfonic groups as an interesting perspective for heterogeneous acid-catalysis [35]. After treating the thiol modified colloidal particles with H_2O_2 20% v/v for 1 day at room temperature, a signal was observed at 169.1 eV corresponding to SO_3H groups [36] (see supplementary information).

4. Conclusions

We have demonstrated the selective modification of pores in a mesoporous colloidal SiO_2 particle at room temperature. Co-hydrolysis of TEOS with MPTMS in the presence of a porogen such as CTAB resulted in multiple porous layers which determine different chemical environments for specific purposes [11b]. XPS has shown the possibility to localize functional chemical groups in different layers. In this context, the synthesis of hybrid layered colloids with highly functional organic frameworks stand as an attractive platform for localized chemistry, active sensing and smart catalytical materials [37,38].

Acknowledgments

A.W., M.G., A.V.B., F.W. and H.T are members of CONICET. We thank Dr. M. Jobbágy and K. Kabuto for assistance with XRD measurements. Funding was provided by ANPCYT PICT 00392, PIP CONICET 11220090101031 and GABBOS.

Appendix A. Supplementary materials

Supplementary data associated with this article can be found in the online version at doi:10.1016/j.jssc.2011.12.028.

References

[1] F. Caruso, Colloids and Colloid Assemblies—Synthesis, Modification, Organization and Utilization of Colloid Particles, Wiley-VCH, Weinheim, 2003.
[2] H. Wang, D.W. Brandl, P. Nordlander, N.J. Halas, Acc. Chem. Res. 40 (2007) 53–62.
[3] D. Van Gough, A. Wolosiuk, P.V. Braun, Nano Lett. 9 (2009) 1994–1998.
[4] S.H. Cho, H.M. Andersson, S.R. White, N.R. Sottos, P.V. Braun, Adv. Mater. 18 (2006) 997.
[5] T.A. Berfield, H.K. Patel, R.G. Shimmin, P.V. Braun, J. Lambros, N.R. Sottos, Small 2 (2006) 631–635.
[6] S. Armini, C.M. Whelan, K. Maex, J.L. Hernandez, M. Moinpour, J. Electrochem. Soc. 154 (2007) H667–H671.
[7] B. Städler, R. Chandrawati, K. Goldie, F. Caruso, Langmuir 25 (2009) 6725–6732.
[8] J. Liu, F. Liu, K. Gao, J.S. Wu, D.F. Xue, J. Mater. Chem. 19 (2009) 6073–6084.
[9] M. Kim, K. Sohn, H. Bin Na, T. Hyeon, Nano Lett. 2 (2002) 1383–1387.
[10] A. Calvo, B. Yameen, F.J. Williams, O. Azzaroni, G.J.A.A. Soler-Illia, Chem. Commun. (2009) 2553.
[11] (a) M.C. Fuertes, S. Colodrero, G. Lozano, A.R. Gonzalez-Elipe, D. Grosso, C. Boissiere, C. Sanchez, G. Soler-Illia, H. Miguez, J. Phys. Chem. C 112 (2008) 3157–3163;
(b) M.C. Fuertes, M. Marchena, M.C. Marchi, A. Wolosiuk, G. Soler-Illia, Small 5 (2009) 272–280.
[12] S. Areva, C. Boissiere, D. Grosso, T. Asakawa, C. Sanchez, M. Linden, Chem. Commun. (2004) 1630–1631.
[13] (a) A.J. Bard, Integrated Chemical Systems: A Chemical Approach to Nanotechnology, Wiley, New York, 1994;
(b) C.S.S.R. Kumar, Mixed Metal Nanomaterials, Wiley-VCH, Weinheim, 2009.
[14] (a) C. Park, K. Oh, S.C. Lee, C. Kim, Angew. Chem.-Int. Ed. 46 (2007) 1455–1457;
(b) V. Cauda, A. Schlossbauer, J. Kecht, A. Zürner, T. Bein, J. Am. Chem. Soc. 131 (2009) 11361–11370.
[15] A. Bernardos, E. Aznar, M.D. Marcos, R. Martínez-Máñez, F. Sancenón, J. Soto, J.M. Barat, P. Amorós, Angew. Chem.-Int. Ed. 48 (2009) 5884–5887.
[16] (a) Special issue on Theranostic nanomedicine, Acc. Chem. Res. 44 (10) (2011) and references therein;
(b) S. Angelos, Y.W. Yang, K. Patel, J.F. Stoddart, J.I. Zink, Angew. Chem. Int. Ed. 47 (2008) 2222–2226;
(c) T.D. Nguyen, K.C.F. Leung, M. Liong, Y. Liu, J.F. Stoddart, J.I. Zink, Adv. Funct. Mater. 17 (2007) 2101–2110.
[17] G. Buchel, K.K. Unger, A. Matsumoto, K. Tsutsumi, Adv. Mater. 10 (1998) 1036.
[18] A. Lopez-Noriega, E. Ruiz-Hernandez, S.M. Stevens, D. Arcos, M.W. Anderson, O. Terasaki, M. Vallet-Regi, Chem. Mater. 21 (2009) 18–20.
[19] (a) D. Brühwiler, Nanoscale 2 (2010) 887–892;
(b) H.E. Bergna, W.O. Roberts, Colloidal Silica: Fundamentals and Applications, CRC Press, Boca Raton, 2006.
[20] S.B. Yoon, J.Y. Kim, J.H. Kim, Y.J. Park, K.R. Yoon, S.K. Park, J.S. Yu, J. Mater. Chem. 17 (2007) 1758–1761.
[21] H. Blas, M. Save, P. Pasetto, C. Boissiere, C. Sanchez, B. Charleux, Langmuir 24 (2008) 13132–13137.
[22] W. Stöber, A. Fink, E. Bohn, J. Colloid Interface Sci. 26 (1968) 6269.
[23] M. Hartmann, Chem. Mater. 17 (2005) 4577–4593.
[24] (a) M. Ohmori, E. Matijević, J. Colloid Interface Sci. 150 (1992) 594–598;
(b) W.P. Hsu, R. Yu, E. Matijević, J. Colloid Interface Sci. 156 (1993) 56–65;
(c) A. Guerrero-Martínez, J. Pérez-Juste, L.M. Liz-Marzán, Adv. Mater. 22 (2010) 1182–1195.
[25] P.S. Goyal, B.A. Dasannacharya, V.K. Kelkar, C. Manohar, K. Srinivasa Rao, B.S. Valaulikar, Phys. B: Phys. Condens. Matter 174 (1991) 196–199.
[26] (a) C.E. Fowler, D. Khushalani, B. Lebeau, S. Mann, Adv. Mater. 13 (2001) 649;
(b) B. Tan, S.E. Rankin, J. Phys. Chem. B 108 (2004) 20122;
(c) T. Nakamura, M. Mizutani, H. Nozaki, N. Suzuki, K. Yano, J. Phys. Chem. C 111 (2007) 1093.
[27] Y. Deng, D. Qi, C. Deng, X. Zhang, D. Zhao, J. Am. Chem. Soc. 130 (2008) 28–29.
[28] J.C. Vartuli, K.D. Schmitt, C.T. Kresge, W.J. Roth, M.E. Leonowicz, S.B. McCullen, S.D. Hellring, J.S. Beck, J.L. Schlenker, Chem. Mater. 6 (1994) 2317–2326.
[29] K. Yano, T. Nakamura, Chem. Lett. 35 (2006) 1014–1015.
[30] (a) D. Son, A. Wolosiuk, P.V. Braun, Chem. Mater. 21 (2009) 628–634;
(b) A. Zelcer, A. Wolosiuk, G. Soler-Illia, J. Mater. Chem. 19 (2009) 4191–4196.
[31] (a) P. Yang, D. Zhao, D.I. Margolese, B.F. Chmelka, G.D. Stucky, Nature 396 (1998) 152–155;
(b) C.T. Kresge, M.E. Leonowicz, W.J. Roth, J.C. Vartuli, Nature 359 (1992) 710–712.

[32] P.C. Angelomé, L. Andrini, M.E. Calvo, F.G. Requejo, S.A. Bilmes, G.J.A.A. Soler-Illia, J. Phys. Chem. C 111 (2007) 10886–10893.
[33] (a) R.M. Almeida, C.G. Pântano, J. Appl. Phys. 68 (1990) 4225;
(b) M.D. Sacks, T.-Y. Tseng, J. Am. Ceram. Soc. 67 (1984) 532;
(c) A. Burneau, O. Barrès, J.P. Gallas, J.C. Lavalley, Langmuir 6 (1990) 1364.
[34] A. Calvo, P.C. Angelomé, V.M. Sánchez, D.A. Scherlis, F.J. Williams, G.J.A.A. Soler-Illia, Chem. Mater. 20 (2008) 4661–4668.
[35] E. Cano-Serrano, G. Blanco-Brieva, J.M. Campos-Martin, J.L.G. Fierro, Langmuir 19 (2003) 7621–7627.
[36] A. Walcarius, V. Ganesan, Langmuir 22 (2006) 469–477.
[37] T.M. Suzuki, T. Nakamura, E. Sudo, Y. Akimoto, K. Yano, J. Catal. 258 (2008) 265–272.
[38] M. Mizutani, Y. Yamada, T. Nakamura, K. Yano, Chem. Mater. 20 (2008) 4777–4782.